Hollow Three-dimensional Model for Fuel Reduction in Aviation Industry

Siva Marimuthu[1*], Manikandan Natarajan[2], Ramesh R[2], Rajadurai Murugesan[3]

[1]Department of Engineering, Staffordshire University, Stoke on Trent, United Kingdom.

[2]Department of Mechanical Engineering, Sree Vidyanikethan Engineering College, Tirupati, India.

[3]Department of Aeronautical Engineering, NITTE Meenakshi Institute of Technology, Bangalore, India.

Abstract

In the past two years, the pandemic situation has affected the aviation industry drastically. This situation starts to change, gradually, which is about to highly increase the international air travel around the world. Commercial air transport emission contributes a significant amount to global warming. Hence, in this research, to reduce the fuel consumption in commercial aircraft the aerodynamic surface of the wing is improved with the help of a hollow model in three dimensions. This biomimetic model named Raw Riblet was derived from a shark's skin texture. The cross-section of the wing was (NACA 0012) designed and the Raw Riblet model was implemented in two different ways, computationally, and formulated biomimetic aerofoil models such as BRR and LRR (0.455). All these aerofoil models were analysed in high-speed airflow, computationally, and the aerodynamic performance values were noted. All the computational results were validated, and the result analysis showed a promising decrease in viscous drag of up to 11%. Both biomimetic models performed well in disturbance reduction when compared to the NACA model. This improved aerodynamic surface with reduced drag would decrease the fuel consumption in aircraft. This computational model would help us to fight the war against global warming.

Keywords: *Aerofoil; Biomimetics; Computational Fluid Dynamics; Transonic flow; Viscous reduction.*

Abbreviations:

B – Bottom

HPBA – Hollow Patterned Biomimetic Aerofoil

L – Low-depth

NACA – National Advisory Committee for Aeronautics

RR – Raw Riblet

3D – Three Dimension

1. Introduction

The European Union has planned to reduce aviation emissions up to 75% by 2050 [1]. In relation to that, many European countries have invested their funds to develop a sustainable solution for emission reduction. Much research was done on alternate powered aircraft, idea was to switch the propulsion from gas turbine engines to solar power, battery electric power, and so on [2]. However, these solutions couldn't compensate the long-range commercial aircraft which require more energy for operation. Hence, we are again back to square one i.e., finding a way to improve the emission of available aircraft models in large use. This made the way for the necessity to improve the aerodynamic surface of a commercial aircraft. The main aerodynamic surface of any aircraft is the wing which generates lift force by keeping the flow disturbances at bay. These disturbances are called drag which increases at high angles of wing operation which would lead to high fuel consumption and emission, accordingly. Drag is of many types such as friction, induced, after-body, interference, wave, and parasitic. Out of which friction contributes to the maximum amount of total drag in commercial aircraft [3]. Therefore, it is essential to reduce the friction drag which improves the efficiency [4].

Friction drag is also called viscous drag which occurs due to the interaction between the wing surface and the fluid particles. Jianlong et al, noted in their research that with the increase in the angle of attack, the disturbance around the NACA 0012 would increase [5]. Although there are many ways to reduce that, biomimetic is the most promising approach in recent times [6, 7]. Biomimetics is a way of finding solutions to problems in engineering sciences from nature [8, 9]. Even in viscous drag reduction biomimetic sets a new pathway. Studies on shortfin mako sharks (as shown in Figure 1) revealed that the riblets are aligned in the direction of fluid flows, which reduces the interaction between the skin surface and the fluids [10]. Bechert and Reif proved the idea of shark skin drag reduction up to 3% [11]. Bhatia et al, analysed two models using computational fluid dynamics and noted a 4% reduction in drag [12]. Similarly, Wen et al fabricated a 3D printed shark skin and tested it in fluid flow which reduced the speed of the object to 6% [13]. Sharkskin pattern was also implemented in the internal pipeline flow and the drag reduction was noted as high as 7% [14]. Han et al. made a biomimetic pattern using a different manufacturing technique and investigated it in the fluid flow which reduced the drag to 8% [15]. Dai et al. concluded at the end of their flow studies that the 3D pattern sharkskin would reduce the drag up to 9 % [16]. Zhang et al. developed a computational model of shark skin pattern and verified the computational results with the experimental values which

evidenced from 8% to 9.5% in drag reduction [17]. Therefore, in this research work, a biomimetic pattern was developed from shark skin and implemented on a smooth aerofoil surface in two different ways. It was then studied in computational fluid flow which resulted in improved the performance of the aerodynamic surface.

2. Computational Model

From the scanning electron microscopic image of the Carcharhinus Falciformis as shown in Figure 1(a), dimensions are obtained. Apart from the microscopic dimensions, specifications such as height and thickness were scaled to the length ratio and designed a Raw Riblet (RR) model in three dimensions as shown in Figure 1(b), computationally, using the Solidworks software because of its effectiveness [18] in part design. The RR pattern was designed very similar to the sharkskin which helped in fluid flow disturbance reduction.

(a)
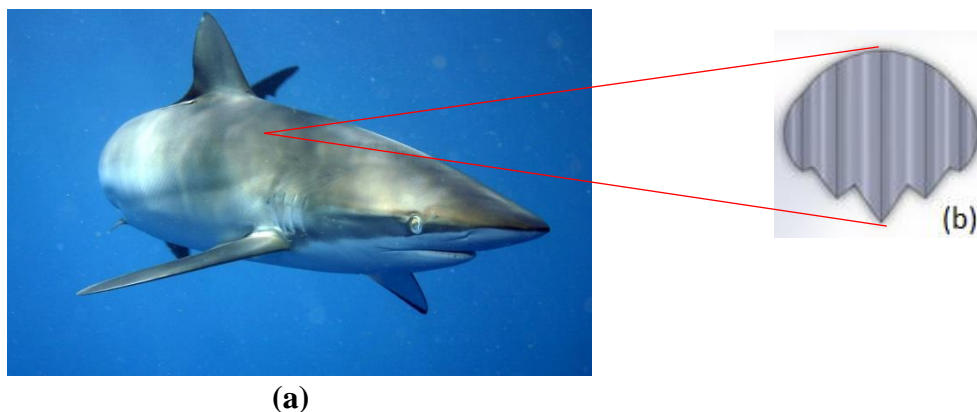
**Figure 1. (a) Carcharhinus Falciformis – Silky Shark [19],
(b) 3D design of Raw Riblet [20, 21]**

In order to design an aerodynamic surface, the most common symmetrical aerofoil structure named NACA 0012 was taken into account. Based on the coordinates obtained from airfoiltools.com, a NACA 0012 wing was modelled in three dimensions using Solidworks as shown in Figure 2(a). The fluid disturbances usually occur at the leading edge and flow downstream of the surface. Hence, to reduce the drag in those areas, the RR pattern was placed at the bottom (downstream) and near to the lead edge of the NACA 0012 aerofoil, separately. These models are called biomimetic models. Due to the implementation of a hollow pattern at the bottom and low-depth locations, these models are called bottom raw riblet (BRR) and low-depth raw riblet (LRR) models as shown in Figure 2(b) and 2(c), respectively. The depth of the

pattern in the LRR and BRR models are 0.455 and 0.5 metres, respectively. The chord length of the NACA model is 1 metre. NACA and biomimetic models were saved as the solid part file type which helped in computational analysis.
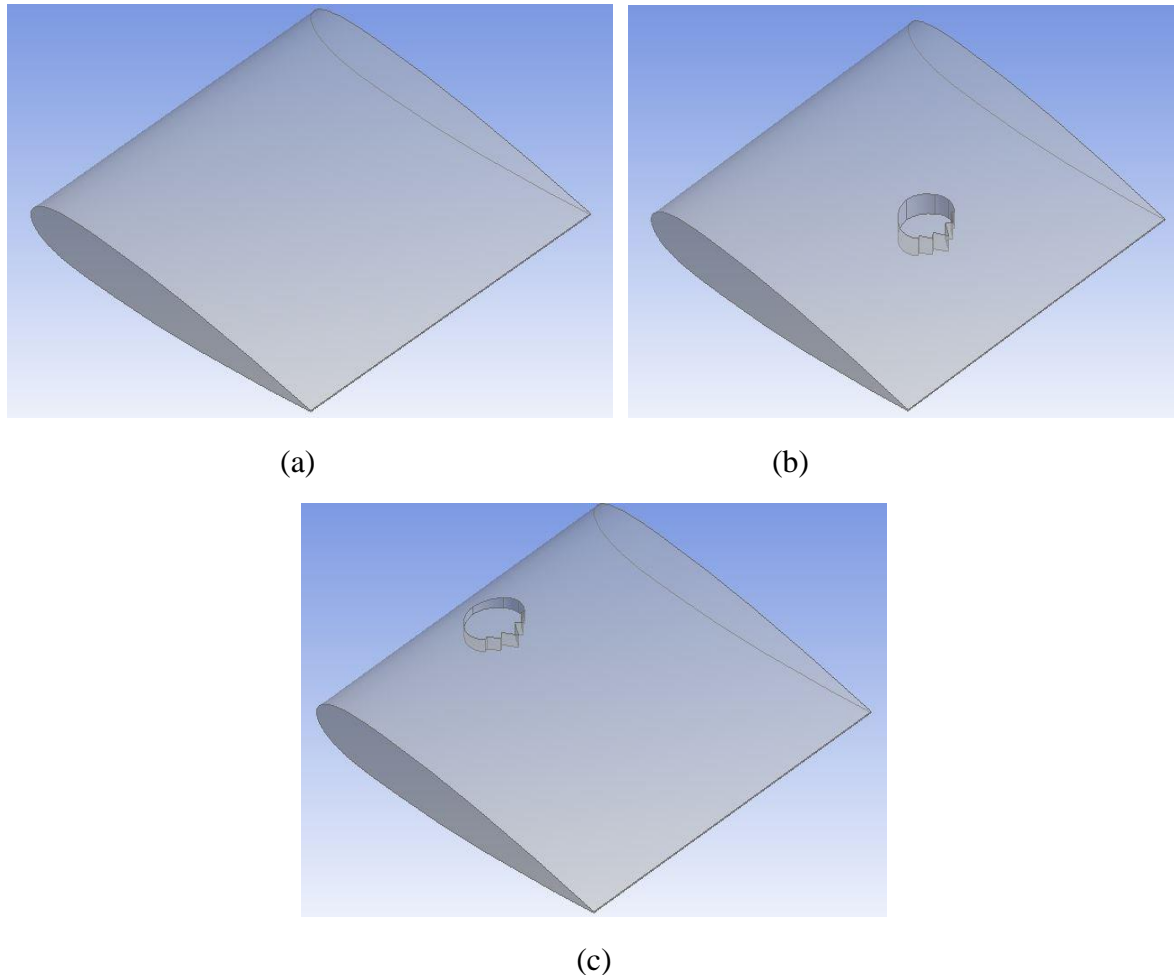

Figure 3. (a) NACA 0012 [16], (b) 1BRR HPBA, (c) 1LRR(0.455) HPBA

3. Computational Analysis

ANSYS is a user-friendly commercial tool that works well in both external and internal fluid flow analysis [22]. Therefore, the 3D computational models were imported onto the Design Modeler of the ANSYS. In this section, a computational domain was formulated with respect to the scaling ratio of an experimental wind tunnel and chord length of the models, individually. The target and tool-bodies were defined at the end.

The NACA and biomimetic aerofoil models were imported into the Mesh section of the ANSYS-Fluent. In this section, all the faces of the models were divided into many parts and the boundary conditions were set such as inlets, outlets, walls, etc, separately. It was then meshed using the default mesh option, which divided the solid into many small units called cells or grids or elements with nodes. This would help us to apply and solve the governing equations for every cell, individually. The meshed models were checked for any errors and saved. These models were then imported into Fluent. In this section, the qualities of the meshed models were checked. Additionally, the tetrahedral mesh elements were converted into the polyhedral mesh as shown in Figure 3 which would help to reduce the computational time by approximating the gradients of each cell and their neighbours. Sosnowski concluded in the research that polyhedral mesh would give accurate results at a less computational cost [23]. The Sutherland law was enabled for its effectiveness. Most of the long-range commercial aircraft fly at high subsonic Mach numbers between 0.6 to 0.9 [24]. This is a compressible flow regime where the viscous drag is predominant. Hence, in this research, 0.8 Mach airflow was considered to investigate which is within the transonic flow regime. The gauge pressure was calculated with the use of below mentioned formulae.

$$\frac{P_0}{P} = \left(\frac{1+(\gamma-1)}{2}M^2\right)^{\frac{\gamma}{\gamma-1}} = 66471 \text{ Pascal [20]}$$

where P_0- Total pressure (101325 pa), P – Static pressure, γ – Gas constant (1.4), M- Mach number (0.8). Spalart Allmaras – a one equation model opted for its effectiveness in external fluid flow investigations. The SA model is given using the following equation.

$$\frac{\partial \hat{v}}{\partial t} + u_j \frac{\partial \hat{v}}{\partial x_j} = c_{b1}(1 - f_{t2})\hat{S}\hat{v} - \left[c_{w1}f_w - \frac{c_{b1}}{k^2} f_{t2}\right]\left(\frac{\hat{v}}{d}\right)^2 + \frac{1}{\sigma}\left[\frac{\partial}{\partial x_j}\left((v + \hat{v})\frac{\partial \hat{v}}{\partial x_j}\right) + c_{b2}\frac{\partial \hat{v}}{\partial x_i}\frac{\partial \hat{v}}{\partial x_i}\right]$$

Where, $\hat{S} = \Omega + \left[\frac{\hat{v}}{k^2 d^2} f_{v2}\right]$, $\Omega = \sqrt{2W_{ij}W_{ij}}$ is the magnitude of the vortices, d is the distance from the field point to the nearest wall, $f_w = g\left[\frac{1+c_{w3}^6}{g^6+c_{w3}^6}\right]^{\frac{1}{6}}$, $g = r + c_{w2}(r^6 - r)$, $r = \min\left[\frac{\hat{v}}{\hat{S}k^2 d^2}, 10\right]$, $f_{t2} = c_{t3}\exp(-c_{t4}x^2)$, $W_{ij} = \frac{1}{2}\left(\frac{\partial u_i}{\partial x_j} - \frac{\partial u_j}{\partial x_i}\right)$. The boundary conditions are: $\hat{v}$ for wall = 0, $\hat{v}$ for far field = $3v_\infty$: to: $5v_\infty$. Note that these boundary conditions on the Spalart Allmaras turbulence field variable correspond to turbulent kinematic viscosity values

of: v^t for far field = $0.210438v_\infty$: to ： $1.294234v_\infty$. The constants are: $C_{b1} = 0.1355$, $\sigma = $ $2/3$, $C_{b2} = 0.622$, $k = 0.41$, $C_{w2} = 0.3$, $C_{w3} = 2$, $C_{v1} = 7.1$, $C_{t3} = 1.2$, $C_{t4} = 0.5$, $c_{w1} = \frac{c_{b1}}{k^2} + \frac{1+c_{b2}}{\sigma}$ [25]. Ideal gas law was chosen for its properties. Second-order equations and coupled solution methods were chosen which helped to solve the models in transonic flow. The solution was initialized from the inlet and iterated at 0^0, 3^0, 6^0, 9^0, 12^0, 15^0, 18^0, 21^0, 24^0, 27^0, 30^0 angles of attack.
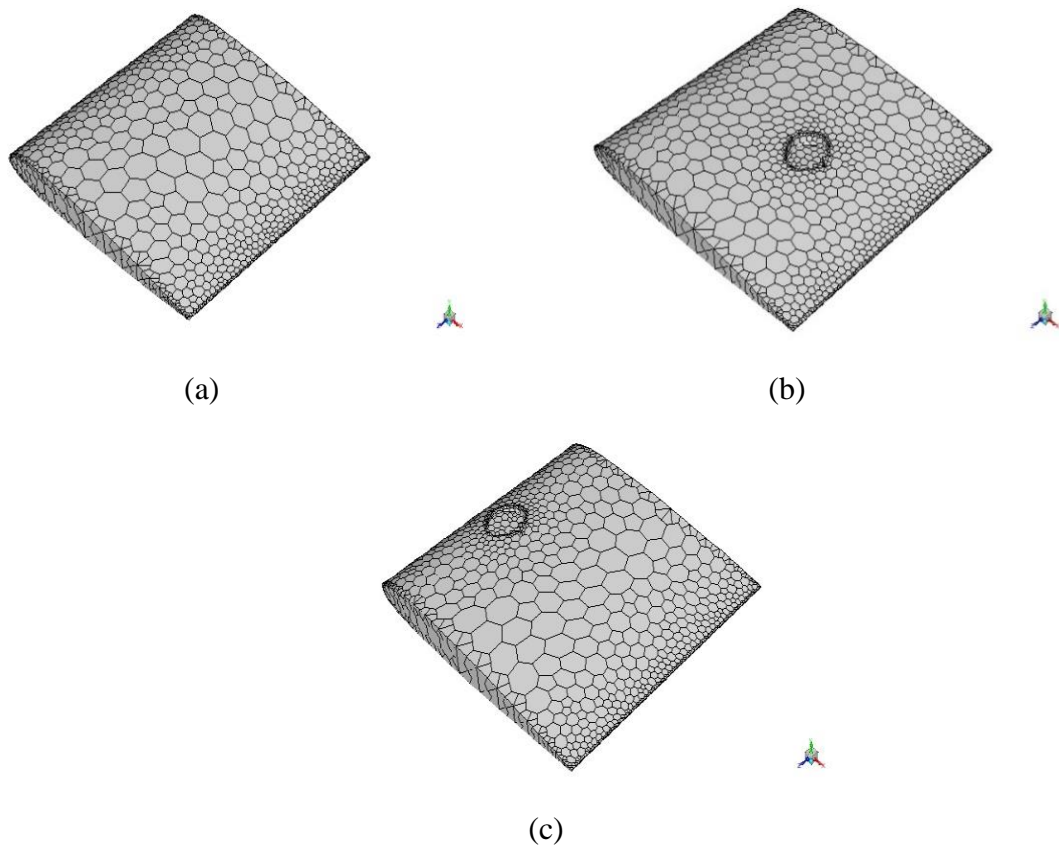

(a)

(b)

(c)

Figure 3. Polyhedral Mesh image of; (a) NACA 0012, (b) 1BRR, and (c) 1LRR (0.455).

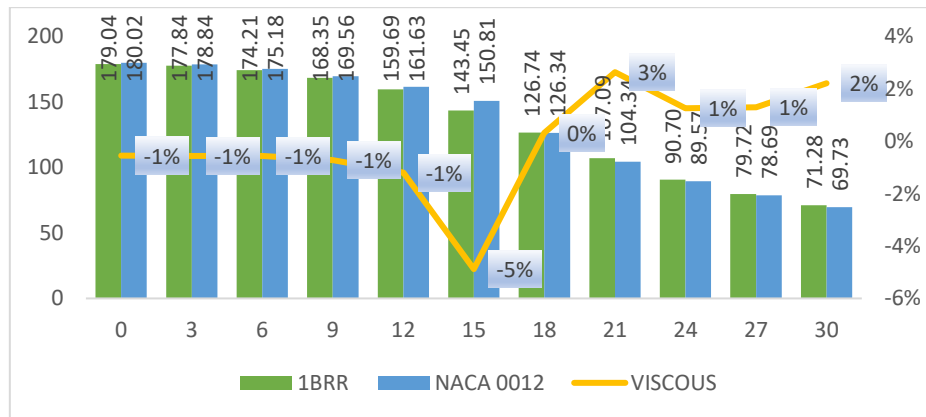## 4. Results and Discussion

4.1 NACA 0012 Vs 1-BRR HPBA

Figure 4. NACA 0012 Vs 1BRR: Viscous drag

Figure 4, clearly shows that the viscous drag force of 1BRR HPBA varied from 179.04 N at 0^0 to 71.28 N at 30^0 angles of attack. Similarly, the viscous drag of NACA 0012 varied from 180.02 N at 0^0 to 69.73 N at 30^0. At 0^0, 3^0, 6^0, 9^0 and 12^0 angles of attack, the variation between the two models is near to -1%. Whereas, at 18^0, 21^0, 24^0, 27^0, and 30^0 angles of attack, the viscous forces vary from 0 to 3%. Based on the comparison between these models, 1BRR performed better from 0^0 to 15^0 angles of attack when compared to the NACA 0012. The viscous drag reduction was as high as 5% at 15^0 angle of attack.
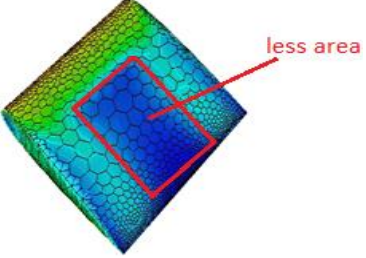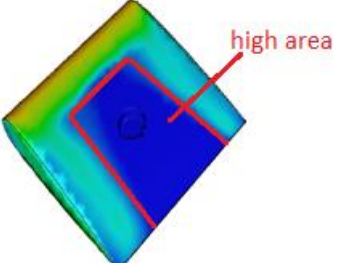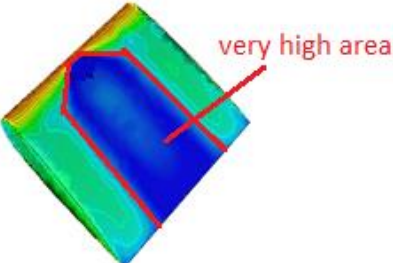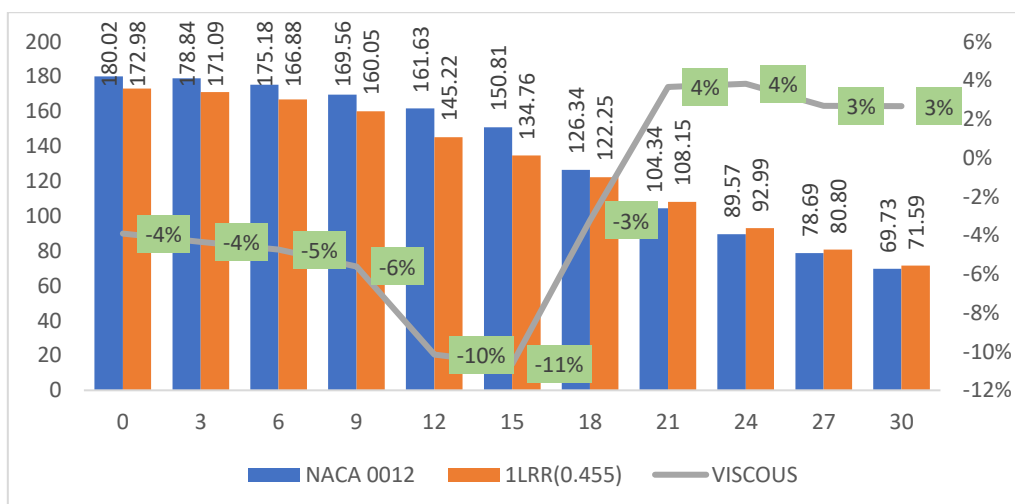
4.2 NACA 0012 Vs 1-LRR (0.455) HPBA

Figure 5. NACA 0012 Vs 1LRR (0.455): Viscous drag

Figure 5, clearly shows that the viscous drag force of 1LRR (0.455) HPBA varied from 172.98 N at 0^0 to 71.59 N at 30^0 angles of attack. Similarly, the viscous drag of NACA 0012 varied from 180.02 N at 0^0 to 69.73 N at 30^0. At 0^0, 3^0 and 18^0 angles of attack, the variation between the two models is between -3 and -4%. Whereas, at 6^0, 9^0 and 12^0 angles of attack, the variation between the two models is between -5 and -10%. At 21^0, 24^0, 27^0 and 30^0, angles of attack the variation between the two models is between 3 and 4%. Based on the comparison between these models, 1LRR (0.455) performed better from 0^0 to 18^0 angles of attack when compared to the NACA 0012. The viscous drag reduction was as high as 11% at 15^0 angle of attack.

4.3 NACA0012 Vs 1BRR Vs 1LRR (0.455)

Although both biomimetic models performed better than NACA 0012 in viscous drag reduction, 1LRR (0.455) reduced the viscous drag higher than that of the 1BRR model. The reason is elaborated in Table 1.

Table 1. Skin-friction Coefficient

Models at 15^0	Explanation
(a) NACA 0012	The skin-friction coefficient distribution on the wall surface of the NACA 0012 shows that the area with reduced values of the skin-friction coefficient is less.
(b) 1BRR HPBA	1BRR HPBA model's surface contour of skin friction coefficient demonstrates that the values of skin friction could be reduced at large with the implementation of the RR pattern in the downstream position.
(c) 1LRR (0.455) HPBA	Due to the application of the RR pattern near to the leading edge, in 1LRR (0.455) skin friction coefficient is reduced at very large areas on the aerofoil surface. Hence, 1LRR (0.455) achieved a higher amount viscous drag reduction.

4.4 Validation

The grid refinement test proved that the values were validated against Gregory's experimental values and the mesh element size is reliable as shown in Table 2. When the NACA 0012 model meshed with a size of 0.49, the coefficient of lift varied highly. Similarly, the mesh element size of 0.51 resulted in negative values of the lift coefficient. The lift and drag coefficients obtained at 0.5 element size were in close agreement with Gregory's experimental values. Due to the values at 0.5 being within the tolerance level, the same element size was used in this research for computational analysis.

Table 2. Validation

Mesh Element Size	Coefficient of lift	Coefficient of drag
0.49	0.0002	0.019
0.50	**0.001**	**0.019**
0.51	-0.00005	0.0195
Experimental Values [26]	**0.005**	**0.017**

5. Conclusion

At high angles of attack, the reversed fluid flow enters into the hollow chamber of the RR model. These fluid particles would circulate within the hollow section, circulate above the aerofoil surface and straighten which would run in parallel to the mainstream flow [17]. This reduced the interaction between the fluids and surface which improved drag, eventually. This RR computational model is very promising in reducing the disturbances in the transonic flow regime as high as 15%. This would reduce fuel consumption greatly in long-range air transportation which reduces global emissions. Further research recommended exploring this surface pattern experimentally.

6. References

1. European Commission, Flightpath 2050 Europe's Vision for Aviation Report of the High-Level Group on Aviation Research, Luxemberg, 2011.
2. More Electric Aircraft, Next Generation Aircraft Power, 2019.

3. Gowree, E. R., Influence of Attachment Line Flow on Form Drag, Thesis, 2014.

4. Kumar, S., Pandey, K. M., Sharma, K. K., Advances in drag-reduction methods related with boundary layer control – A review, Materials Today: Proceedings, 45 (7), 6694-6701, 2021.

5. Jianlong, C., Qingui, Z., Liujing, H., Yi, Zhou., Shedding vortex characteristics analysis of NACA 0012 airfoil at low Reynolds numbers, Energy Reports, 8(4), pp.156-174, 2022.

6. Yu, C., Liu, M., Zhang, C., Yan, H., Zhang, M., Wu, Q., Liu, M., Lei, J., Bio-inspired Drag Reduction from Nature: Organisms to Artificial Functional, Giant, 2, 100017, 2020.

7. Liu, G., Yuan, Z., Qiu, Z., Feng, S., Xie, Y., Leng, D., Tian, X., A Brief Review of Bio-Inspired Surface Technology and Application Toward Underwater Drag Reduction, Ocean Engineering, 199, 106962, 2020.

8. Siva, M., Rajadurai, M., Pandyrajan, R., and Babu.B, Design of Dragon Fly Aircraft, Research Inventy: International Journal of Engineering and Science, 2(10), 40-47, 2013.

9. Siva, M., Megalingam Murugan, A., Sivasathya U., and Dharmalingam, S., Biomimetic in Turbulence Reduction – Recent Developments, Journal of Applied Sciences Research, 11(19), 123-134, 2015.

10. Lang, A.W., Bradshaw, M. T., Smith J. A., Wheelus, J. N., Motta, P. J., Habegger, M. L., Hueter, R. E., Movable Shark Scales Act as a Passive Dynamic Micro-Roghness to Control Flow Separation, Bioinspired, Biomimetic and Nanobiomaterials, 9(3), 036017, 2014.

11. Bechert, D. W., Reif, W. E., On the Drag Reduction of the Shark Skin, in: AIAA Shear Flow Control Conference, 85-0546, 1-8, 1985.

12. Bhatia, D., Zhao, Y., Yadav, D., Wang, J., Drag Reduction Using Biomimetic Sharkskin Denticles, Engineering, Technology & Applied Science Research, 11 (5), 7665 – 7672, 2021.

13. Wen, L., Weaver, J.C., Lauder, G.V., Biomimetic Shark Skin: Design, Fabrication and Hydrodynamic Function, J. Exp. Biol. 217 (10), 1656-1666, 2014.

14. Liu, K. N., Christodoulou, C., Riccius, O., Joseph, D. D., Drag Reduction in Pipes Lined with Riblets, AIAA J. 28 (10), 1697-1698, 1990.

15. Han, X., Zhang, D., Li, X., Li, Y., Bio-replicated Forming of the Biomimetic Drag Reducing Surfaces in Large Area based on Shark Skin, Chin. Sci. Bull. 53 (10), 1587-1592, 2008.

16. Dai, W., Alkahtani, M., Hemmer, P. R., Liang, H., Drag Reduction of 3D Printed Shark Skin Like Surfaces, Friction, 7(6), 603-612, 2019.

17. Zhang, D., Luo, Y., Li, X., Chen, H., Numerical Simulation and Experimental Study of Drag Reducing Surface of a Real Shark Skin, Journal of Hydrodynamics, 23 (2), 204-211, 2011.

18. Ragoth S. R., Nataraj, M., Surendar, S., Siva, M., Investigation of a centrifugal pump impeller vane profile using CFD, International Review on Modelling and Simulations, 6 (4), 1327-1333, 2013.

19. https://upload.wikimedia.org/wikipedia/commons/9/9f/Carcharhinus_falciformis_off_ Cuba.jpg., Accessed 2021.

20. Siva Marimuthu., and Dhavamani Chinnathambi., Computational Analysis to Enhance the Compressible Flow over an Aerofoil surface, Aircraft Engineering and Aerospace Technology, 93(5), 925-934, 2021.

21. Marimuthu, S., Al-Rabeei, S., Boha, H.A., Three-Dimensional Analysis of Biomimetic Aerofoil in Transonic Flow, Biomimetics, 7, 20, 2022.

22. Siva Marimuthu., and Dhavamani Chinnathambi., Computational Analysis of Biomimetic Butterfly Valve, Bioinspired, Biomimetic and Nanobiomaterials, 9(4), 223-232, 2020.

23. Sosnowski, M., Krzywanski, J., Grabowska, K., & Gnatowska, R., Polyhedral meshing in numerical analysis of conjugate heat transfer, EPJ Web of Conferences, 180, 02096, 2018.

24. https://www.paramountbusinessjets.com/aviation-terminology/mach-number.html#:~:text=Most%20airliners%20currently%20travel%20around,starts%20to%20form%20shock%20waves., Accessed 2022.

25. Siva, M., Computational investigation of biomimetic surface pattern to enhance the fluid flow over a surface, Thesis, Anna University, Chennai, 2021.

26. Gregory, N., Wilby, P.G., NPL 9615 and NACA 0012 A Comparison of Aerodynamic Data, Ministry of Defense, Aerodynamic Division, NPL, Her Majesty's Stationery Office, London, 1973.